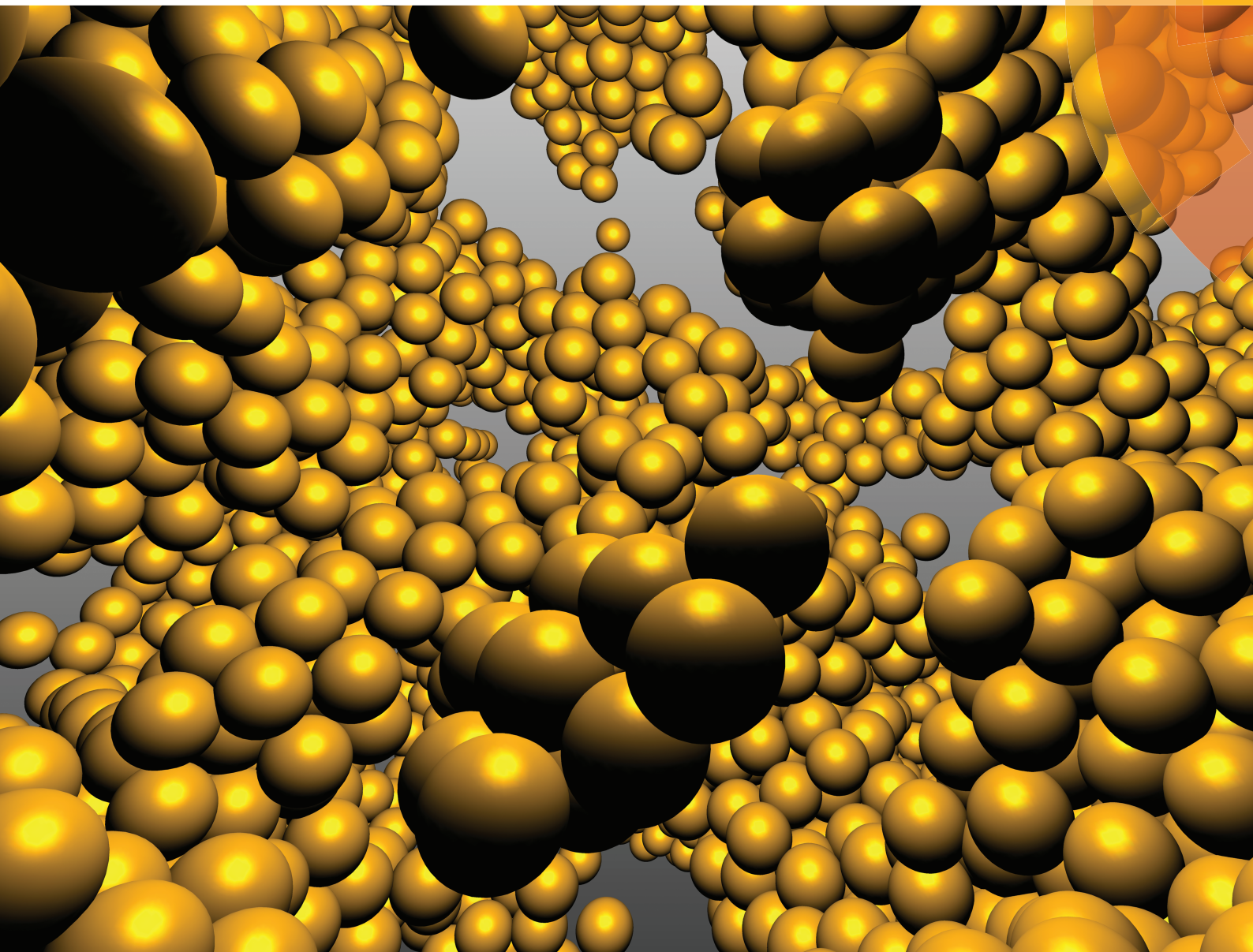


Soft Matter

www.softmatter.org



ISSN 1744-683X



PAPER

Vasileios Prymidis *et al.*
Self-assembly of active attractive spheres



Cite this: *Soft Matter*, 2015, 11, 4158

Received 16th January 2015,
Accepted 24th March 2015

DOI: 10.1039/c5sm00127g

www.rsc.org/softmatter

Self-assembly of active attractive spheres†

Vasileios Prymidis,* Harmen Sielcken and Laura Filion

We study the self-assembly of a system of self-propelled, Lennard-Jones particles using Brownian dynamics simulations. We examine the state diagrams of the system for different rotational diffusion coefficients of the self-propelled motion of the particles. For fast rotational diffusion, the state diagram exhibits a strong similarity to that of the equilibrium Lennard-Jones fluid. As we decrease the rotational diffusion coefficient, the state diagram is slowly transformed. Specifically, the liquid–gas coexistence region is gradually replaced by a highly dynamic percolating network state. We find significant local alignment of the particles in the percolating network state despite the absence of aligning interactions, and propose a simple mechanism to justify the formation of this novel state.

1. Introduction

In recent years a significant amount of research has been focused on active matter systems, whose individual units are able to convert internal energy or energy from the local environment into their own motion (see ref. 1–4 for recent reviews). This focus was boosted by important experimental advances in the synthesis of artificial swimmers and walkers on the colloidal and granular scale,^{5–14} and the possible link between the behaviour of these man-made systems and the collective motion of living organisms (for example swimming cells or bacteria).^{15,16} Active systems show a plethora of exotic phenomena such as giant density fluctuations,^{9,17} vortex formation,^{11,18} and swarming.¹¹ Moreover, they may play an important role in useful future applications such as targeted cargo delivery and novel types of materials.^{19–21}

However, even though experimentalists gain increasingly better control over the realization of active systems, the physics community lacks a fundamental understanding of the laws that govern their collective behavior. Thus, it comes as no surprise that a substantial amount of research is devoted to seemingly simple theoretical models of active particles, with the Viscek model being possibly the most studied one.^{22,23} Another much studied example, more related to the colloidal world, is the system of self-propelled, hard or purely repulsive disks.²⁴ Computer simulations and continuum models have established that this active fluid phase-separates into a dense and a dilute region for sufficiently fast swimming velocities.^{24–28} Even though the phase-separation of self-propelled disks can partially be linked

with the clustering of particles reported in many experiments,^{13,29,30} there has not yet been a satisfying explanation for the latter phenomenon, as the interactions between the colloids are more complex than simple steric interactions.³¹

A simple step towards complexity is the addition of attractive interactions between the particles, which was shown to also lead to clustering of particles. Specifically, Palacci *et al.* showed in a numerical study that phoretic attraction between self-propelled hard disks gives qualitative agreement between the clustering properties of their model and their experiments.¹³ A more elaborate numerical study on the interplay between attraction and self-propulsion was done by Redner *et al.*³² The authors studied a two-dimensional ensemble of self-propelled particles that interact *via* Lennard-Jones interactions. By varying the strength of the attraction and the swimming velocity of the particles, they showed that the self-propulsion can have two opposing effects for a given strength of attraction – for slow swimmers it can break aggregations caused by the attractive force, while it can induce aggregation for fast enough swimmers. For intermediate swimming velocities, the steady state of the system was identified as a homogeneous fluid phase. A first study of a similar model in three dimensions has been done by Moggetti *et al.*³³ The focus of this work was mainly on the clustering properties of the system – as the strength of attraction is increased, the system passes from a homogeneous state to a clustered state caused by the attractive interactions. A state of rotating clusters has also been reported in ref. 34 for active attractive dumbbells.

However, the transition from homogeneity to clustering in active attractive systems has not yet been clearly linked with the known phase behaviour of the corresponding equilibrium systems. Moreover, structural properties of the clustered state have not been examined and compared to the well-studied gas–liquid phase separation.

Soft Condensed Matter, Debye Institute for Nanomaterials Science, Utrecht University, Princetonplein 5, 3584 CC Utrecht, The Netherlands.
E-mail: v.prymidis@uu.nl

† Electronic supplementary information (ESI) available. See DOI: 10.1039/c5sm00127g



In the present work we study a three-dimensional model of self-propelled Brownian particles that interact *via* a Lennard-Jones potential. The choice of the potential qualitatively accounts for the steric repulsion and the short range attraction that are present in many colloidal systems. By tuning the rotational diffusion rate of the particles, we are able to continuously move the system from the regime of fast rotational diffusion, where strong similarities with the equilibrium behavior are expected,³⁵ to small values of the diffusion rate where non-equilibrium features arise. Thus, we are able to construct a series of state diagrams that evolve from a diagram similar to the well-established Lennard-Jones phase diagram to diagrams with novel properties.

Moreover, we find that the interplay between attraction and self-propulsive motion in three dimensions gives rise to a highly dynamic, percolating network. As we will show in this paper, this percolating network has many similarities to living clusters, observed in ref. 33. It is, however, a system spanning structure. This new state is accompanied by an unexpected result – the emergence of local alignment of the axes of self-propulsion of the particles despite the absence of an aligning mechanism.

In Section II we describe the model, the dynamics implemented for our simulations and the analysis methods used in the subsequent parts of the article. In Section IIIA we present the state diagrams of the system, and in IIIB we focus on properties of the percolating network state. Lastly, we compare our work with the results of ref. 33 in Section IIIC and give a short discussion of our results in Section IV.

II. Methods

A. Model

In this paper we examine the behaviour of self-propelled, attractive particles immersed in a solvent. We consider a three-dimensional system, consisting of spherical particles (colloids) in a periodic cubic box of length L . The position of the center of mass of the i th particle at time t is given by the vector $\vec{r}_i(t)$. To each particle i , we associate a three-dimensional unit vector $\hat{p}_i(t)$ that identifies the direction in which the self-propelling force propels the particle at a given time. The particles interact with each other *via* a Lennard-Jones potential

$$\beta U(r_{ij}) = 4\beta\epsilon \left[\left(\frac{\sigma}{r_{ij}} \right)^{12} - \left(\frac{\sigma}{r_{ij}} \right)^6 \right], \quad (1)$$

truncated and shifted at 2.5σ , where σ is the particle length scale, $r_{ij} = |\vec{r}_j - \vec{r}_i|$, ϵ is the strength of the interaction and $\beta = \frac{1}{k_B T}$ is the inverse temperature of the system, with k_B the Boltzmann constant and T the temperature.

B. Dynamics

We do not model the solvent explicitly, but rather only include it implicitly. We use two distinct expressions to describe the translational motion of the individual colloidal particles inside

the solvent, namely the underdamped and overdamped Langevin equations. The underdamped Langevin equation is given by

$$m \frac{d^2 \vec{r}_i}{dt^2} = - \sum_{j \neq i} \frac{\partial U(r_{ij})}{\partial \vec{r}_i} - m\gamma \frac{d\vec{r}_i}{dt} + F_p \hat{p}_i + \sqrt{\frac{2m\gamma}{\beta}} \vec{\bar{A}}_i^{\text{tr}}, \quad (2)$$

where m is the particle's mass, γ is the damping coefficient and F_p denotes the magnitude of the self-propelling force. Note that $\vec{\bar{A}}_i^{\text{tr}}$ is a unit-variance random vector, with mean value and variation

$$\langle \vec{\bar{A}}_i^{\text{tr}}(t) \rangle = 0 \quad (3)$$

$$\langle \vec{\bar{A}}_i^{\text{tr}}(t) \vec{\bar{A}}_j^{\text{tr}}(t') \rangle = \mathbb{I}_3 \delta_{ij} \delta(t - t'), \quad (4)$$

where \mathbb{I}_3 is the unit matrix in three dimensions. The forces that appear on the right-hand side of eqn (2) are, from left to right, the force due to particle interactions, the drag force, the self-propelling force and a stochastic force. The drag and stochastic forces account for the constant collisions between the colloidal particles and the molecules of the solvent.

In the regime of low Reynolds numbers (typical of a colloidal system) one can neglect the inertial term, and thus the translational motion of each particle follows from the overdamped Langevin equation

$$\frac{d\vec{r}_i}{dt} = \beta D_{\text{tr}} \left[- \sum_{j \neq i} \frac{\partial U(r_{ij})}{\partial \vec{r}_i} + F_p \hat{p}_i \right] + \sqrt{2D_{\text{tr}}} \vec{\bar{A}}_i^{\text{tr}}, \quad (5)$$

where the translational diffusion coefficient is given by the Einstein–Smoluchowski relation $D_{\text{tr}} = 1/(\beta m \gamma)$. We define the unit of time $\tau = \sigma^2 D_{\text{tr}}^{-1}$.

The axis of self-propulsion is subject to rotational diffusion and in our simulations its motion always obeys the overdamped rotational Langevin equation

$$\frac{d\hat{p}_i}{dt} = \sqrt{2D_r} (\hat{p}_i \times \vec{\bar{A}}_i^{\text{r}}), \quad (6)$$

where D_r denotes the rotational diffusion coefficient and the random vector $\vec{\bar{A}}_i^{\text{r}}$ satisfies relations analogous to eqn (3) and (4). For spherical particles in the low-Reynolds number regime, the translational and rotational diffusion coefficients are linked *via* the Stokes–Einstein relation $D_r = 3D_{\text{tr}}/\sigma^2$. Nevertheless, the rotational diffusion coefficient is considered as an independent parameter in our study, similar to previous theoretical work.^{35–37} The reason for this extra degree of freedom is that individual particles in experimental active systems, such as bacterial colonies,¹⁵ are often subject to athermal rotational diffusion.

In order to implement the aforementioned equations of motion eqn (5) and (6) we used the Euler–Maruyama integration scheme.³⁸ To implement the underdamped Langevin eqn (2), we employed the integration scheme proposed by Grønbech-Jensen and Farago.³⁹ We have verified that simulations in the overdamped regime give indistinguishable results with ones in the highly viscous underdamped regime. A time step of $dt = 3 \times 10^{-5} \tau$ was used for the numeric integration of the equations of motion and the simulations ran for at least $10^6 \tau$, so that we get sufficient statistics for the system.



The behavior of the system was probed as the following dimensionless parameters were systematically varied: the strength of the Lennard-Jones potential $\tilde{\epsilon} = \beta\epsilon$, the magnitude of the propulsion force $\tilde{F} = \beta F_p \sigma$, the rotational diffusion coefficient $D_r \tau$ and the density of the system $\rho \sigma^3 = \frac{N \sigma^3}{L^3}$. In the case of the underdamped system, we also varied the (dimensionless) damping coefficient $\tilde{\gamma} = \beta m \gamma \sigma^2 / \tau$. Following ref. 33, we quantified the ratio between the strength of attraction and the magnitude of self-propulsion by the aggregation propensity

$$P_{\text{agg}} = \frac{\tilde{\epsilon}}{\tilde{F}} = \frac{\epsilon}{F \sigma}. \quad (7)$$

The number of particles for all simulations in the underdamped regime was 1728, in order to compare directly our results with ref. 33, while for the overdamped regime it was 4917, unless stated otherwise. The effects of the finite size of the system on our results are discussed, when considered relevant, in the next section.

C. Steady state and initial configurations

Due to the self-propelling force there is constant energy input in the system. Nevertheless, by following the evolution of the total potential energy of the system with time, we observed that after a short transient period there was no energy drift. After this period the potential energy of the system fluctuated around a mean value. We identified this regime of quasi-constant energy with the steady state of the system. For our measurements we considered configurations from the steady state only. Furthermore, for each point in the parameter space, a minimum of two simulations was performed, starting from two different initial configurations: one where the particles were on a cubic lattice that spanned the entire system, and one where all the particles were part of a dense liquid slab. These two initial conditions were chosen in order to study any possible effect the starting configuration could have on the steady state of the system. We found that after the transient period, the average potential energy in both simulations converged to the same value, which indicates that the system indeed relaxed at the same state and we can safely identify the regime of quasi-constant potential energy with the steady state. For a limited number of simulations we also looked at the time evolution of the degree of clustering and the local density histograms, both of which are described in detail later in this paper, and we found that in the regime of quasi-constant energy these structural functions were also only subject to fluctuations and there were no major changes. Once again the results obtained for different initial configurations coincided. All the above ensure that potential energy is a reasonable indicator of when the system reaches the steady state.

For sets of parameters where the system is close to crystallization, the system was additionally initialized from a gaseous state that contains a large (face-centered-cubic) crystalline cluster. The cluster contained approximately 25% of the system's particles. We observed high crystallization and melting barriers in many cases, which caused difficulties in identifying the true

state of the system, as the simulations would have to run for a very long time. We found that these difficulties were enhanced by finite size effects. Nevertheless, the results obtained for the parameter space points presented in this article have been thoroughly verified.

D. Analysis methods

We used a Voronoi construction to construct local density histograms of the system.⁴⁰ By calculating the volume of the Voronoi cells we were able to estimate the local density of particles. Furthermore, the identification of surface particles was performed by means of the cone algorithm.⁴¹

In order to distinguish the percolating network state from the bulk gas-liquid coexistence region we used the following criterion. First, we considered two particles as clustered when their center of mass distance was less than 1.2σ . Note that in our system, the first minimum in the radial distribution function is typically between 1.3σ and 1.6σ . We chose 1.2σ as the cutoff distance in order to both be consistent with that used in ref. 33 and ensure that we did not overestimate the amount of connectedness in our system.

Second, we calculated the probability of having a cluster percolating simultaneously in all three dimensions in the system. To determine whether a cluster percolates in a given direction we duplicated the system in that direction, doubling the number of particles. If the number of particles in the cluster doubled as well, then the cluster percolated. When the probability of percolation was found higher than a certain threshold that was density-dependent, we identified the system as being in the percolating cluster state. This threshold was used for the necessary distinction between strong fluctuations of the liquid phase that can temporarily percolate in three dimensions and the percolating network structure. The probability threshold was set at 35%, 90% and 95% for total densities $\rho \sigma^3 = 0.191$, 0.382 and 0.445 accordingly. However, for a total density higher than $\rho \sigma^3 = 0.5$ this criterion failed as the liquid cluster always percolated.

III. Results

A. State diagrams

Passive Lennard-Jones particles have been extensively studied and their phase behaviour is well-characterized (see *e.g.* ref. 42). At high temperatures, Lennard-Jones systems exhibit a single first-order phase transition from a fluid to a face-centered-cubic crystal as the density of the system is increased. Upon lowering the temperature, a critical temperature is reached where a second phase transition appears separating the fluid phase into gas and liquid phases. At even lower temperatures a triple point appears below which the liquid phase disappears and only the gas and crystal remain.

When the passive particles are replaced by active particles by introducing self-propulsion, deviations from the equilibrium behaviour are expected. To explore these deviations, we study the behaviour of the system as a function of the rotational diffusion coefficient $D_r \tau$ while keeping the self-propulsion force and temperature fixed. Note that in the limit of fast rotational



diffusion, $D_r\tau \rightarrow \infty$, the persistence length of the particles goes to zero and the active force acts effectively as translational diffusion.³⁵ As a result, we expect the behaviour in this limit to coincide with the behaviour in the equilibrium (passive) system, but with a modified interaction strength. However, as $D_r\tau$ is decreased, the non-equilibrium effects should become more evident.

In this section we use overdamped Brownian dynamics simulations to explore the behaviour of systems with $D_r\tau$ between 0.3 and 30 and densities $\rho\sigma^3$ between 0.191 and 0.764. In all cases, the magnitude of the self-propelling force is fixed at $\tilde{F} = 50$.

For all values of $D_r\tau$ we consider, we find that the system forms a homogeneous fluid for a sufficiently low value of $\tilde{\epsilon}$ (see Fig. 1(a)). As the strength of the attraction is increased, the particles tend to aggregate. The structure of the aggregate depends strongly on the rotational diffusion coefficient. For a high rotational diffusion coefficient, the aggregated phase appears as the liquid in a classical liquid–gas phase separation, namely, the liquid phase is organized such that the surface of the cluster is minimal (Fig. 1(b)). However, for slower rotational diffusion, the aggregated phase is much less compact as shown in Fig. 1(c), and frequently spans the entire system or forms “living” clusters as described in ref. 33.

In order to better quantify the aggregation of particles, we obtained density histograms for the systems we examined. We found that in most cases the density histograms transitioned from a unimodal to a bimodal curve as the strength of attraction is increased, a transition that indicates passing from a homogeneous state into a coexistence state. Examples of such histograms are presented in Fig. 2. We subsequently used the local maxima of the density histograms, which we identified as the local densities of the coexisting phases ρ_l , to construct the state diagram of the system for different rotational diffusion coefficients, see Fig. 3. Note that in Fig. 2 some of the peaks in

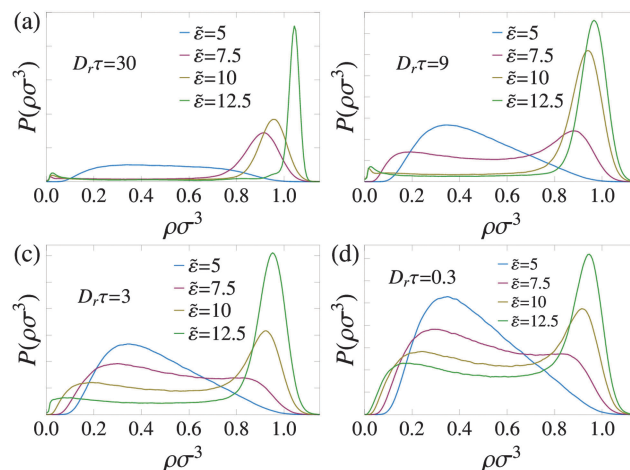


Fig. 2 Local density histograms for a system with total density $\rho\sigma^3 = 0.381$ and magnitude of self-propulsion $\tilde{F} = 50$. $P(\rho\sigma^3)$ denotes the probability to find a particle with local density $\rho\sigma^3$. The subfigures (a)–(d) correspond to different rotational diffusion coefficients as indicated.

the gas phase are very low compared to the peaks of the liquid phase, indicating that only a small fraction of our system consisted of gas particles. We identified as fluid the state where only a single peak is visible in the local density histogram. States which exhibited two peaks but showed no signs of global phase separation were identified as percolating network states, and states which exhibited a clear phase separation were marked as either gas–liquid or gas–crystal, depending on whether the high density phase is crystalline. Note that we have not probed the exact positions of the critical or triple points in any of the diagrams presented in Fig. 3. Additionally, the boundaries presented in black dashed lines are simply approximate state boundaries.

As shown in Fig. 3(a), for a rotational diffusion coefficient $D_r\tau = 30$ (ten times larger than the value dictated by the Stokes–Einstein relation), the behaviour of the system is very similar to the phase diagram seen for passive systems. The system transitions with increasing attractive strength $\tilde{\epsilon}$ from a homogeneous fluid state to a gas–liquid coexistence state and eventually to a gas–crystal coexistence state. Moreover, the binodal envelope is similar to that of the equilibrium system, in the sense that the value of attraction alone dictates the densities of the two coexisting phases. The low-density curves do not fall exactly on top of each other for high values of attraction due to surface effects that are discussed at the end of this section.

Decreasing the rotational diffusion to $D_r\tau = 9$ (Fig. 3(b)) results in the emergence of a new state, which we refer to as a percolating network. This new state consists of a dynamic network of clustered particles coexisting with a gas phase and in static images resembles an equilibrium system which has undergone spinodal decomposition (see the ESI† Movie S1). However, in contrast to such a state, the percolating network we observe is clearly not kinetically trapped (see the ESI† Movie S2). From Fig. 3(b) we see that the system now transitions with increasing strength of attraction from a homogeneous fluid state to a percolating network and then to a gas–liquid coexistence state.

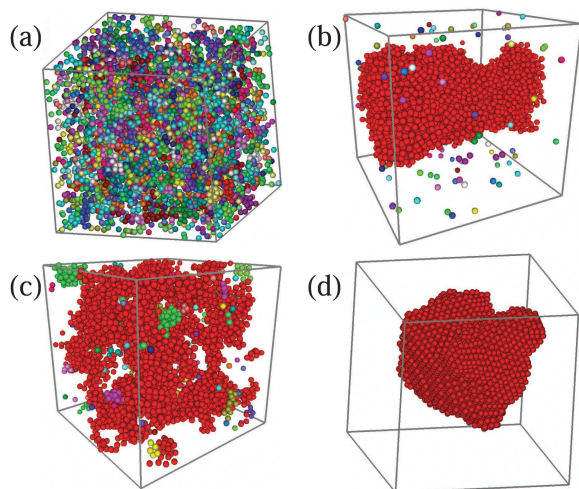


Fig. 1 Snapshots of different states of the system. In (a) the system is in a homogeneous fluid state, in (b) there is liquid–gas coexistence, in (c) a percolating network state is found, and in (d) a crystal coexists with a gas. Particles that belong to different clusters have different colours. The values of the parameters are $\rho\sigma^3 = 0.191$, $\tilde{F} = 50$, $\tilde{\epsilon} = 5$, for (a) and 12.5 for (b)–(d) and $D_r\tau = 30, 4.2, 0.01$, and 30 for (a)–(d) respectively.



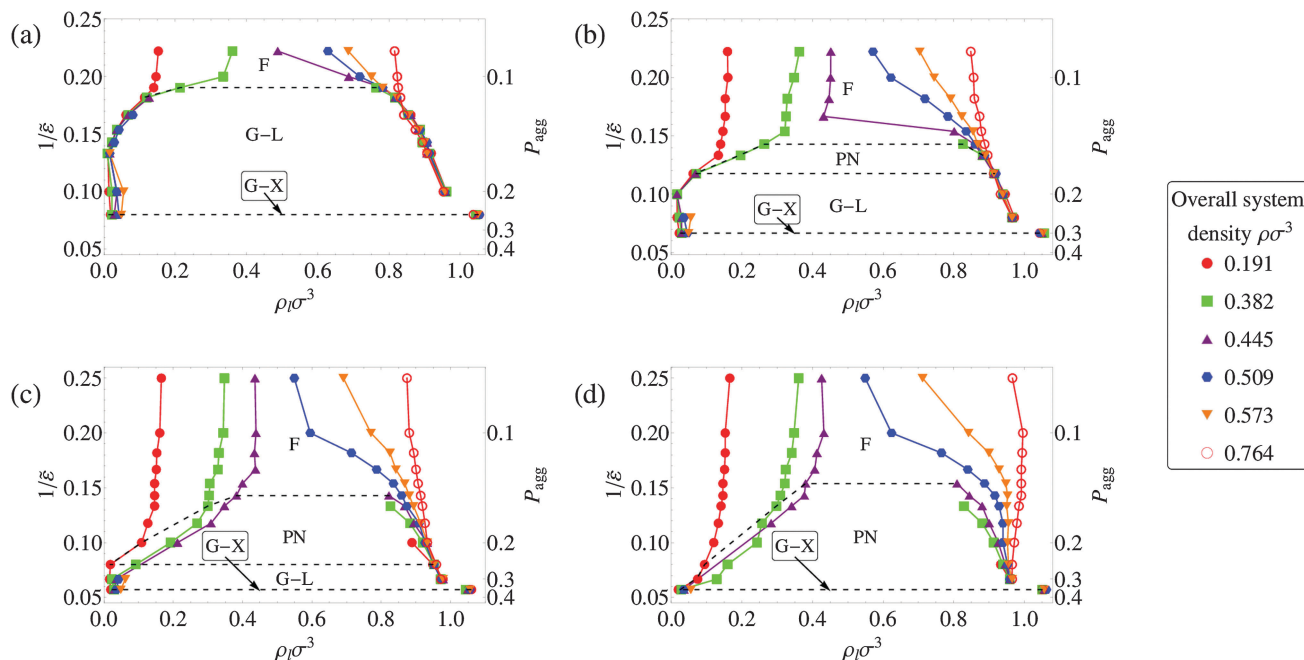


Fig. 3 (a)–(d) State diagrams of the active Lennard-Jones system with rotational diffusion coefficients $D_r\tau = 30, 9, 3$, and 0.3 respectively. On the y-axis $1/\bar{\epsilon} = k_B T/\bar{\epsilon}$ denotes the inverse attraction strength of the system and $P_{\text{agg}} = \bar{\epsilon}/\bar{F}$ is the aggregation propensity. Data points correspond to local maxima of density histograms, which we identify as the local densities ρ_l of the coexisting phases. Different symbols correspond to different overall densities of the system. The black dashed lines indicate approximate state boundaries. Labels are as follows: F indicates the fluid, G–L gas–liquid coexistence, G–X gas–crystal coexistence and PN the percolating network state.

Setting the rotational diffusion coefficient equal to the value dictated by the Stokes–Einstein relation, namely $D_r\tau = 3$, results in the state diagram shown in Fig. 3(c). Here, we find that the region where the percolating network state occurs is increased at the expense of the gas–liquid coexistence region. Additionally, in the percolating network region, attraction does not solely dictate the densities of the coexisting states anymore. In contrast, the peaks in the local density histograms also depend on the total density of the system. We note that this non-collapse was validated for various system sizes as described below.

For very low rotational diffusion ($D_r\tau = 0.3$), the state diagram continues to evolve (Fig. 3(d)). The percolating network has now completely replaced the gas–liquid region – according to our simulations, the system transitions directly from the percolating network state to a gas–crystal coexistence state.

Interestingly, the stability domain of the percolating network increases monotonously with decreasing rotational diffusion coefficient. In all investigated cases, it appears first at $1/\bar{\epsilon} \approx 0.15$, with the value increasing slightly with decreasing $D_r\tau$.

We conclude this section by commenting on finite size effects. In order to ensure that the behaviour we observed in Fig. 3 was robust with respect to the system size, we simulated a few state points for larger and smaller systems, consisting of $N = 21\,952$ and 2197 particles respectively. First of all, we found that the identification of the states does not change, *e.g.* we observe fluid, liquid–gas, crystal and the percolating network independent of system size. Additionally, the density of the dense phase (percolating network of liquid clusters, liquid or crystal) was only slightly affected by the system size. Substantial

deviations occurred only for the low-density phase. These deviations are expected, since the first peak of the local density histogram is complicated by the presence of surface particles in addition to the gas particles. Nevertheless, this effect does not affect the conclusions drawn above.

B. Percolating cluster state

One of the most striking differences between a gas–liquid coexistence state and the novel percolating network state is the compactness of the dense clusters. In a gas–liquid coexistence state, the system evolves in order to minimize the surface area of the cluster, resulting in compact spherical or cylindrical geometries. In the percolating network, the active system appears to almost attempt to maximize the surface area, resulting in a highly branched network. One way to characterize this difference is by looking at the ratio of surface to volume of these large aggregates. In Fig. 4 we plot the average ratio N_s/N_v of surface particles over the total number of particles for the largest cluster, as a function of the rotational diffusion coefficient. In all cases, the density $\rho\sigma^3 = 0.191$, self-propelling force $\bar{F} = 50$ and interaction strength $\bar{\epsilon} = 12.5$ are chosen such that nearly all particles are part of one large cluster ($>90\%$). We have found that for the parameters used in Fig. 4 the fluctuations of the number of particles in the biggest cluster N_v as well as of the ratio N_s/N_v are small. Thus, the size of the largest cluster does not fluctuate significantly, and the dynamic changes in the shape of the percolating network do not seem to affect the presented results.

In the fast rotational diffusion regime, the liquid cluster is indeed compact, resulting in a small surface-to-volume ratio,



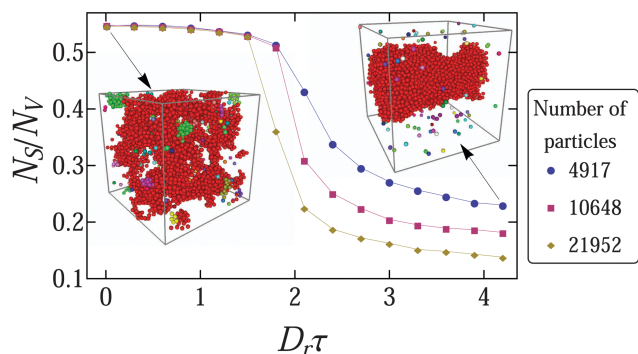


Fig. 4 Average ratio of the number of surface particles N_s over the number of particles N_v in the biggest cluster of the system, as a function of the rotational diffusion coefficient $D_r\tau$. For all points, $\tilde{F} = 50$, $\tilde{\epsilon} = 12.5$, and $\rho\sigma^3 = 0.191$. The insets show snapshots of the system for the corresponding values of $D_r\tau$. Particles that belong to different clusters have different colours.

which decreases further with increasing system size, as expected. On the other hand, for low rotational diffusion, *i.e.* in the percolating network state, we observe a much larger fraction of surface particles, which is independent of the system size. For the system parameters studied in Fig. 4 we find that the transition between the network state and the gas-liquid separation occurs at a rotational diffusion of around $D_r\tau \sim 2$. Note that this transition becomes sharper with increasing system size, characteristic of a phase transition.

To gain further insight into the properties of the percolating network state, we study the pairwise correlations between particles. In Fig. 5(a), we plot the radial distribution function $g(r)$ for four different values of $D_r\tau$, at the same density and interaction strength as was used for Fig. 4. For the highest value of $D_r\tau$, the system exhibits a gas-crystal phase separation, and the radial distribution function shows sharp peaks characteristic of the crystalline order. For $D_r\tau = 9$ and 3, the system forms a gas-liquid separation, resulting in much weaker peaks in $g(r)$. Finally, for $D_r\tau = 0.3$, we observe the percolating network state, for which the radial distribution function looks essentially the same as that of the gas-liquid separation.

Additionally, we calculate the normalized orientation correlation function $C_1(r)$, defined as

$$C_1(r) = \frac{\left\langle \sum_{i=1}^N \sum_{j=1}^N \delta(r - r_{ij}) \hat{p}_i \cdot \hat{p}_j \right\rangle}{\left\langle \sum_{i=1}^N \sum_{j=1}^N \delta(r - r_{ij}) \right\rangle}, \quad (8)$$

where the prime on the summation sign indicates the terms for which $i = j$ are not included. The angular brackets indicate a configurational average. This function is equal to unity if all the axes of self-propulsion of particles are aligned, and equal to zero if all particle orientations are uncorrelated. We plot $C_1(r)$ in Fig. 5(b). In all cases, we see that for $r < \sigma$, there is a negative correlation between the orientations of the particles. This is expected, as the only way for particles to be significantly closer than $r = \sigma$ is for them to be pushing towards each other. Additionally, as expected, the crystalline state shows significant

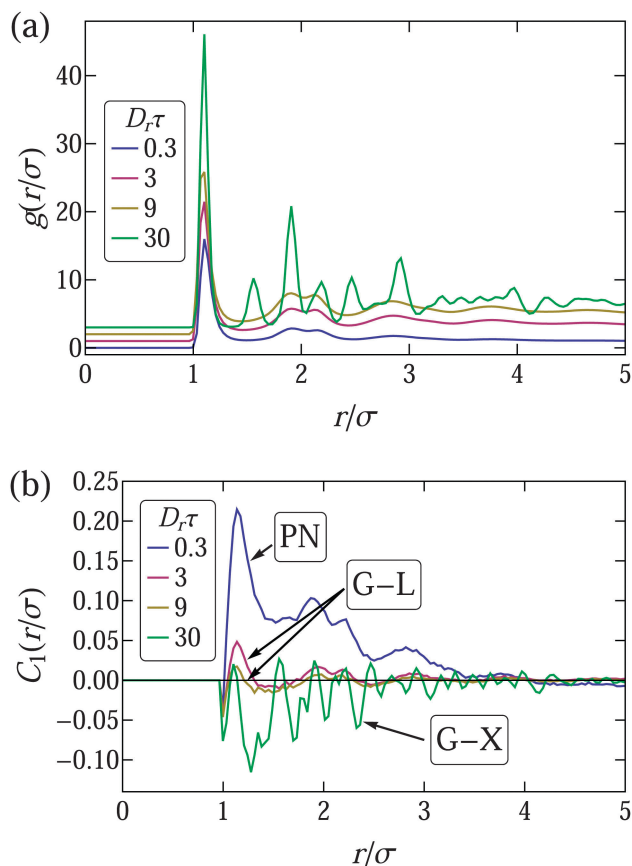


Fig. 5 Radial distribution function $g(r)$ (a), and normalized orientation correlation function $C_1(r)$ (b) for different values of the rotational diffusion coefficient. All curves correspond to values of the parameters $\rho\sigma^3 = 0.191$, $\tilde{F} = 50$, and $\tilde{\epsilon} = 12.5$. For $D_r\tau = 30$, the crystal and the gas coexist, for $D_r\tau = 9$ and 3, the liquid and the gas coexist and for $D_r\tau = 0.3$, the system is in the percolating network state. Note that in figure (a) the radial distribution functions are offset for clarity.

statistical noise, due to small values of the denominator in eqn (8). The most important result in Fig. 5 is the strong local alignment of particles in the percolating state in comparison to the other states. As there is no explicit aligning torque in the model, this is surprising, and indicates that particles with similar orientations tend to stay in closer proximity in the percolating network.

In light of the above conclusions, we propose here a possible mechanism that accounts for the formation of the percolating network state. Consider a dilute system of self-propelled particles with an attraction strength at least strong enough to cause gas-liquid phase separation in the absence of self-propulsion. Now assume that the magnitude of self-propulsion is stronger than the attractions $\tilde{F} > \tilde{\epsilon}$, and that the axis of self-propulsion associated with each particle is pointing in a fixed, random direction ($D_r\tau = 0$). When two particles collide there are two possible scenarios – if their axes of self-propulsion are pointing in a similar direction, then the attraction will cause them to aggregate and travel together. In contrast, if the axes of self-propulsion are pointing in sufficiently different directions, the particles will overcome the attraction and move away from each other. After a large

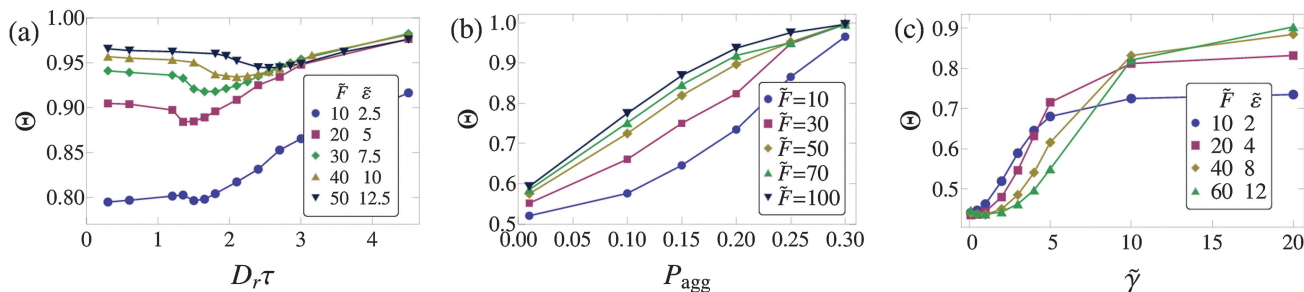


Fig. 6 Degree of clustering Θ as a function of (a) the rotational diffusion coefficient $D_r\tau$ for different values of \tilde{F} and $\tilde{\varepsilon}$, but at a constant ratio $P_{\text{agg}} = 0.25$, (b) P_{agg} for different values of \tilde{F} , and fixed $D_r\tau = 3$ and (c) the dimensionless damping parameter $\tilde{\gamma}$ for different values of \tilde{F} and $\tilde{\varepsilon}$, but at a constant ratio $P_{\text{agg}} = 0.20$ and constant $D_r\tau = 3$. The density of the system is $\rho\sigma^3 = 0.191$, same as in ref. 33.

number of collisions, this process will ultimately create a collection of clusters, with each cluster containing particles with similar orientations. By performing a small number of simulations (not shown in the present article) in very low densities $\rho\sigma^3 = 0.001$ – 0.01 and for $\tilde{F} > \tilde{\varepsilon} > 1$, we have indeed verified that the above process creates a collection of small clusters in which particle orientations are highly correlated.

Now, if we increase the system density and instead of a fixed direction of self-propulsion we allow the particles to slowly rotate (corresponding to a low rotational diffusion coefficient), then this argument should continue to hold, *e.g.* particles that are in similar orientations aggregate more easily than particles pointing in opposite directions. This results in highly dynamic aggregates with groups of particles frequently attaching and detaching, and neighbouring particles displaying high degrees of orientational correlation as seen in Fig. 5. For sufficiently high density (such as those studied in this paper), these aggregates become completely system spanning, and the majority of particles are connected to a single network, as seen in our simulations. This picture agrees well with movies from our simulations (see ESI† Movies S1 and S2) and accounts for both the local alignment of particles (Fig. 5) and the lack of system size dependence of the structural properties of the percolating network (Fig. 4).

As $D_r\tau$ increases, the persistence length of the self-propelled motion of the particles decreases. In this case, the attractive force is able to aggregate particles with larger differences in the orientation of the axes of self-propulsion. This process ultimately leads to a transition to the (bulk) gas–liquid phase coexistence region (Fig. 4). A similar transition from the percolating network state to a gas–liquid coexistence state can take place by fixing the persistence length of the particles and increasing the attraction (Fig. 3(b) and (c)).

C. Clustering properties

In a recent publication, Mognetti *et al.*³³ showed that the aggregation, *i.e.* clustering, in a system of self-propelled attractive particles depended only on the ratio $P_{\text{agg}} = \tilde{\varepsilon}/\tilde{F}$. To examine whether this collapse also occurs in our system, we calculated the degree of clustering Θ , introduced in ref. 33, as

$$\Theta = 1 - \frac{\langle N_{\text{clusters}} \rangle}{N}, \quad (9)$$

where $\langle N_{\text{clusters}} \rangle$ is the average number of clusters in the system. We considered particles clustered when their center of mass distance is less than 1.2σ .³³ Thus, $\Theta \rightarrow 0$ when the system is in the dilute gas phase where $\langle N_{\text{clusters}} \rangle \simeq N$, while $\Theta = 1 - \frac{1}{N} \simeq 1$ when all particles belong to the same cluster. The results are plotted in Fig. 6.

In Fig. 6(a) we plot the degree of clustering Θ as a function of the rotational diffusion coefficient $D_r\tau$ at constant P_{agg} near the percolating network to gas–liquid transition. We do not see a collapse in the degree of clustering here. Similarly, in Fig. 6(b) we do not see a collapse when plotting Θ as a function of P_{agg} at fixed rotational diffusion $D_r\tau$ for a wider range of state points. Finally, we checked to see if the collapse would occur if we use underdamped dynamics in place of overdamped dynamics for the translational degrees of freedom. As shown in Fig. 6(c), we also do not find a value of the damping parameter $\tilde{\gamma}$ for which a collapse occurred. We conclude that the data collapse found by Mognetti *et al.*³³ does not occur in our system. We attribute this discrepancy to the difference in the applied dynamics, and more specifically to the different mechanisms that rotate the particles in the two different systems.

IV. Conclusions and outlook

In the present work, we employed computer simulations to study the self-assembly of a system of self-propelled Brownian particles that interact *via* the truncated and shifted Lennard-Jones potential.

We determined state diagrams of the overdamped system for various rates of rotational diffusion of the self-propelled motion of the particles. We found that for fast rotational diffusion, the properties of the state diagram bore strong similarities to the phase diagram of the equilibrium Lennard-Jones system. However, as the rotational diffusion was decreased, new features arose due to the interplay between self-propulsion and attraction. That is, a new state was observed between the fluid phase and gas–liquid coexistence, which we identified as a highly dynamic, percolating network state. That state consisted of interconnected but mobile clusters that created a system-spanning network. Finally, for slow rotational diffusion the (bulk) gas–liquid coexistence disappeared



and the system transitioned from the percolating network state directly to gas–crystal coexistence.

We subsequently discussed the unique properties of the percolating state, and presented evidence of a transition from gas–liquid to a percolating network with decreasing rotational diffusion. By examining the correlations between the orientations of the axes of self-propulsion of the particles, we found significant local alignment in the percolating state. A possible mechanism was proposed in order to explain the formation of the percolating network.

Finally, we noted that the ratio of the strength of attraction over the magnitude of self-propulsion does not solely characterize our system. This is in contrast to what was found in ref. 33, and may be due to differences in the applied dynamics.

We would like to comment here on the significance of the percolating network state. First, we note once more that this state is caused by the synergy between attraction and self-propulsion, so we expect it to be present in three dimensional systems for a wide variety of attractive potentials and propulsion mechanisms. Moreover, our simulations suggest that this novel state is present for low density systems and experimentally relevant rotational diffusion, so a search for this state in real colloidal systems is feasible. As earlier work has shown, hydrodynamic interactions may also cause local alignment of particles, an effect that may enhance the formation of the percolating network state in experimental systems.⁴³

Last but not least, as demonstrated in Section IIIC, the exact dynamics of a theoretical model are of importance not only for the quantitative but also for the qualitative results it generates. Detailed comparisons between different theoretical models, as well as actual experimental systems, such as ref. 31, are thus extremely valuable and needed, in order to deepen our understanding of active matter systems.

Acknowledgements

V.P. and L.F. acknowledge funding from the Dutch Sector Plan Physics and Chemistry, and L.F. acknowledges funding from a NWO-Veni grant. We thank Wiebke Albrecht, Guido Avisati, Tommaso Comparin and Frank Smalenburg for careful reading of the manuscript.

References

- 1 S. Ramaswamy, *Annu. Rev. Condens. Matter Phys.*, 2010, **1**, 323.
- 2 P. Romanczuk, M. Bär, W. Ebeling, B. Lindner and L. Schimansky-Geier, *Eur. Phys. J.: Spec. Top.*, 2012, **202**, 1.
- 3 M. Marchetti, J. Joanny, S. Ramaswamy, T. Liverpool, J. Prost, M. Rao and R. A. Simha, *Rev. Mod. Phys.*, 2013, **85**, 1143.
- 4 I. S. Aranson, *C. R. Phys.*, 2013, **14**, 518.
- 5 W. F. Paxton, K. C. Kistler, C. C. Olmeda, A. Sen, S. K. St. Angelo, Y. Cao, T. E. Mallouk, P. E. Lammert and V. H. Crespi, *J. Am. Chem. Soc.*, 2004, **126**, 13424.
- 6 R. Dreyfus, J. Baudry, M. L. Roper, M. Fermigier, H. A. Stone and J. Bibette, *Nature*, 2005, **437**, 862.
- 7 J. R. Howse, R. A. Jones, A. J. Ryan, T. Gough, R. Vafabakhsh and R. Golestanian, *Phys. Rev. Lett.*, 2007, **99**, 048102.
- 8 Y. Hong, N. M. Blackman, N. D. Kopp, A. Sen and D. Velegol, *Phys. Rev. Lett.*, 2007, **99**, 178103.
- 9 J. Deseigne, O. Dauchot and H. Chaté, *Phys. Rev. Lett.*, 2010, **105**, 098001.
- 10 A. Kudrolli, G. Lumay, D. Volfson and L. S. Tsimring, *Phys. Rev. Lett.*, 2008, **100**, 058001.
- 11 V. Schaller, C. Weber, C. Semmrich, E. Frey and A. R. Bausch, *Nature*, 2010, **467**, 73.
- 12 G. Volpe, I. Buttinoni, D. Vogt, H.-J. Kümmerer and C. Bechinger, *Soft Matter*, 2011, **7**, 8810.
- 13 J. Palacci, S. Sacanna, A. P. Steinberg, D. J. Pine and P. M. Chaikin, *Science*, 2013, **339**, 936.
- 14 A. Bricard, J.-B. Caussin, N. Desreumaux, O. Dauchot and D. Bartolo, *Nature*, 2013, **503**, 95.
- 15 H. C. Berg, *E. coli in Motion*, Springer, 2004.
- 16 R. Thar and M. Köhl, *FEMS Microbiol. Lett.*, 2005, **246**, 75.
- 17 V. Narayan, S. Ramaswamy and N. Menon, *Science*, 2007, **317**, 105.
- 18 Y. Sumino, K. H. Nagai, Y. Shitaka, D. Tanaka, K. Yoshikawa, H. Chaté and K. Oiwa, *Nature*, 2012, **483**, 448.
- 19 L. Baraban, M. Tasinkevych, M. Popescu, S. Sanchez, S. Dietrich and O. Schmidt, *Soft Matter*, 2011, **8**, 48.
- 20 N. Koumakis, A. Lepore, C. Maggi and R. Di Leonardo, *Nat. Commun.*, 2013, **4**, 2588.
- 21 F. C. Keber, E. Loiseau, T. Sanchez, S. J. DeCamp, L. Giomi, M. J. Bowick, M. C. Marchetti, Z. Dogic and A. R. Bausch, *Science*, 2014, **345**, 1135.
- 22 T. Vicsek, A. Czirók, E. Ben-Jacob, I. Cohen and O. Shochet, *Phys. Rev. Lett.*, 1995, **75**, 1226.
- 23 H. Chaté, F. Ginelli, G. Grégoire and F. Raynaud, *Phys. Rev. E: Stat., Nonlinear, Soft Matter Phys.*, 2008, **77**, 046113.
- 24 Y. Fily and M. C. Marchetti, *Phys. Rev. Lett.*, 2012, **108**, 235702.
- 25 G. S. Redner, M. F. Hagan and A. Baskaran, *Phys. Rev. Lett.*, 2013, **110**, 055701.
- 26 J. Stenhammar, D. Marenduzzo, R. J. Allen and M. E. Cates, *Soft Matter*, 2014, **10**, 1489.
- 27 J. Stenhammar, A. Tiribocchi, R. J. Allen, D. Marenduzzo and M. E. Cates, *Phys. Rev. Lett.*, 2013, **111**, 145702.
- 28 T. Speck, J. Bialké, A. M. Menzel and H. Löwen, *Phys. Rev. Lett.*, 2014, **112**, 218304.
- 29 I. Theurkauff, C. Cottin-Bizonne, J. Palacci, C. Ybert and L. Bocquet, *Phys. Rev. Lett.*, 2012, **108**, 268303.
- 30 I. Buttinoni, J. Bialké, F. Kümmel, H. Löwen, C. Bechinger and T. Speck, *Phys. Rev. Lett.*, 2013, **110**, 238301.
- 31 J. Bialké, T. Speck and H. Löwen, *J. Non-Cryst. Solids*, 2015, **407**, 367.
- 32 G. S. Redner, A. Baskaran and M. F. Hagan, *Phys. Rev. E: Stat., Nonlinear, Soft Matter Phys.*, 2013, **88**, 012305.
- 33 B. M. Mognetti, A. Šarić, S. Angioletti-Uberti, A. Cacciuto, C. Valeriani and D. Frenkel, *Phys. Rev. Lett.*, 2013, **111**, 245702.



- 34 J. Schwarz-Linek, C. Valeriani, A. Cacciuto, M. Cates, D. Maren-duzzo, A. Morozov and W. Poon, *Proc. Natl. Acad. Sci. U. S. A.*, 2012, **109**, 4052.
- 35 Y. Fily, S. Henkes and M. C. Marchetti, *Soft Matter*, 2014, **10**, 2132.
- 36 R. Ni, M. A. C. Stuart and M. Dijkstra, *Nat. Commun.*, 2013, **4**, 2704.
- 37 X. Yang, M. L. Manning and M. C. Marchetti, *Soft Matter*, 2014, **10**, 6477.
- 38 D. Higham, *SIAM Rev.*, 2001, **43**, 525.
- 39 N. Grønbech-Jensen and O. Farago, *Mol. Phys.*, 2013, **111**, 983.
- 40 C. H. Rycroft, *Chaos*, 2009, **19**, 041111.
- 41 Y. Wang, S. Teitel and C. Dellago, *J. Chem. Phys.*, 2005, **122**, 214722.
- 42 B. Smit, *J. Chem. Phys.*, 1992, **96**, 8639.
- 43 I. Llopis and I. Pagonabarraga, *Europhys. Lett.*, 2006, **75**, 999.

